Bachelor Thesis Natuur- en Sterrenkunde

# Characterising the measured intensity within the VULCAN setup

Tomas van der Lee

June 30, 2023

Conducted between April 2023 - June 2023

**Abstract**

Weakly Interacting Massive Particles (WIMPs) are dark matter candidates expected to very rarely interact with xenon. Xenon scintillates when it reacts with a different particle, this property is used in experiments such as XENONnT, which uses a scintillation based Time Projection Chambers (TPCs) to search for these WIMP-xenon interactions. Vacuum Ultraviolet Light Characterisation At Nikhef (VULCAN) looks to further improve our knowledge on materials used in these experiments when interacting with light of the scintillation wavelengths. This thesis characterises the intensity by looking at the necessary corrections, and by looking at the relation between relative intensity and distance, using the VULCAN set up. The relative intensity is calculated by counting the peaks in the traces and by integrating measured voltage over time, to acquire total charge. A quadratic fit is fitted to the relative intensity distance relation with a reduced $\chi^2$ of 3.38 for the counting peaks method and a reduced $\chi^2$ of 7.88 for the integration method.

| | |
|---|---|
| STUDENTNUMBER | 13398091 |
| INSTITUTE | Nikhef |
| RESEARCH GROUP | Dark matter |
| SUPERVISOR | Tina Pollmann |
| DAILY SUPERVISOR | Marjolein van Nuland |
| SECOND EXAMINER | Paul de Jong |

VU VRIJE UNIVERSITEIT AMSTERDAM | UNIVERSITEIT VAN AMSTERDAM

# 1 Populair wetenschappelijke samenvatting

Als we tegenwoordig naar andere sterrenstelsels kijken, kunnen we aan de hoeveelheid licht die wij op aarde kunnen detecteren zien hoeveel massa dat sterrenstelsel heeft. Aan de hand van deze massa kan worden voorspeld hoe sterk de zwaartekracht is en dus hoe snel dit sterrenstelsel om zijn zwaartepunt heen draait. Maar als we kijken naar hoe snel een sterrenstelsel daadwerkelijk draait zien we dat hij veel sneller draait dan zijn massa toestaat. Hoe is dat mogelijk? Het antwoord op deze vraag is nog steeds niet helemaal duidelijk, maar donkere materie zou de oplossing kunnen zijn. Maar wat is donkere materie eigenlijk? Donkere materie is materie, die in tegenstelling tot de materie om ons heen, niet met licht reageert, wat betekent dat we het niet op de bekende manieren kunnen waarnemen. Tegenwoordig zijn er hele grote experimenten die proberen donkere materie waar te nemen door te kijken of het reageert met de stof xenon, als xenon reageert met een ander deeltje komt er namelijk licht van een bepaalde golflengte vrij, dit heet scintilleren. Door hele grote tanks met xenon te vullen en aan de boven en onderkant licht detectoren te plaatsen, zien we het als xenon reageert met een ander deeltje. Alleen hiervoor moeten we wel weten hoe de stoffen waar de detectoren van zijn gemaakt reageren met het licht dat xenon uitzendt tijdens een reactie. Dit is het doel van het VULCAN experiment. het VULCAN experiment schijnt een lamp, die licht uitzendt op de zelfde golflengte waar xenon op scintilleert, op stukjes van de materialen waar de grote detector tanks van zijn gemaakt en meet dan met een kleine licht detector onder andere de reflectiviteit van het materiaal. Binnen het VULCAN experiment heb ik de afgelopen maanden gekeken naar de effecten van verschillende onderdelen van de opstelling op de intensiteit en naar de relatie tussen intenisteit en afstand waarop het wordt gemeten.

# Contents

# 2 Introduction

## 2.1 Origin and strong evidence for dark matter

The term dark matter finds it origin in 1933, when the Swiss astronomer Fritz Zwickie proposed the existence of dark matter to explain the movement of galaxies in the coma cluster [1]. The theory of dark matter has since then helped explain multiple phenomena, with one of the most prominent ones being the rotational velocities of galaxies. When Vera Rubin and Kent Ford were studying the rotational velocities of the Andromeda nebula in 1970, they found that the rotational velocities of stars in the galaxy do not decrease with distance from the galactic center, but stay the same or increase in the outer parts [2]. This discrepancy can be explained by the presence of dark matter, which would provide additional gravitational pull. The findings in [2] are generally viewed as the first proof of dark matter.
Further empirical proof of dark matter was found by Clowe et al. when the galaxy cluster 1E 0657-558, also known as the bullet cluster was investigated [3]. This cluster has two primary concentrations of galaxies that are merging. Because of the merging galaxies the primary baryonic mass component, an X-ray emitting plasma, is slowed down, creating an spatial offset between the plasma and the galaxies in the cluster. The distribution of dark matter is expected to match the galaxy distribution, meaning that if the gravitational potential follows the galaxies instead of the dominant baryonic mass component, the cluster should be dominated by dark matter. Clowe et al. produce gravitational lensing maps in [3] using weak gravitational lensing, these show the potential roughly follows the distribution of galaxies. They found a difference between the total mass center and the center of the visible mass of $8\sigma$ significance, claiming to have found empirical proof of dark matter.
Nowadays dark matter also plays a big role in cosmology, where dark matter is necessary to explain the formation of large structures such as galaxy clusters, superclusters and filaments. The leading cosmological model to explain the current universe is known as the $\Lambda$CDM model or, lambda cold dark matter model, which includes dark matter as a form of matter. This cosmological model was used by the Millenium simulation project [4] to simulate the formation of these large scale structures. In the formation of large scale structures dark matter is gravitationally attracted to the higher density regions seen in the CMB. Making these regions denser, forming the basis of the large scale structures we observe today. During the expansion of the universe these regions served as gravtitational wells accreting more matter, eventually serving as the birth place of galaxies and clusters. The distribution of matter formed a web-like structure, also known as filaments. These filaments are surrounded by voids, which are lower density regions. The Millenium simulation project, simulates the formation of the large scale structures as previously described, and these simulations agree with observations of the current universe, showing dark matter is necessary for the formation of the universe [4].

## 2.2 What is dark matter?

Through extensive research into dark matter, multiple constraints have been put on the nature of the matter, resulting in two main categories, baryonic and non-baryonic dark matter.
Baryonic dark matter refers to matter made up from the same baryons as matter

detectable by telescopes, but it does not emit light, making it non luminous and thus not observable. One type of baryonic dark matter are macho's, macho's are massive compact halo objects, such as rogue black holes or brown dwarfes, that do not emit any light and are not associated with any planetary system. Previous study by P. Tisserand [5] show macho's make up for less then 8% of the halo mass, showing this is not the only source of dark matter.
For the non-baryonic class of dark matter the amount of constraints give us a rough idea what to look for. Observations show that dark matter should be electrically neutral and only have interactions with ordinary matter through the weak nuclear force or gravity [6]. To agree with the theory of giant structure formation that has been previously discussed, dark matter must have been non-relativistic at the time of decoupling, which is also referred to as being cold, giving rise to the cold dark matter model [6]. Dark matter is also expected to have undergone thermal freeze-out in the early universe, leading to an abundance that matches the observed dark matter density if the DM particles are heavy. These together with related arguments have led to the general notion that dark matter is mostly made up of weakly interacting massive particle, also referred to as WIMP.

## 2.3 Dark matter detection

One of the current experiments in search of dark matter in the XENONnT project. This project tries to detect WIMP's through its weak interaction with baryonic matter. A dual-phase xenon time projection chamber (TPC) is build allowing position and energy reconstruction. The TPC is filled with 5.9t of purified liquid xenon. When a particle interacts with the xenon, the liquid scintillates with a wavelength of 178 nm, and it releases ionisation electrons. The primary light flash is detected with arrays of photo multiplier tubes (PMT's) on the top and bottom of the TPC and is called the S1 signal. The released electrons are carried upwards by an electric field reaching the Xenon gas, where a second stronger electric field accelerates the electron creating a second light signal, known as the S2 signal [7]. The position can be reconstructed from the location of the S2 signal and the time between both signals. Energy reconstruction is done by adding the S1 and S2 signal [7]. The detector has two types of background signals known as electronic recoil(ER) and nuclear recoil(NR). Through the S1/S2 ratio there can be easily distinguished between these types of signals, and a WIMP interaction, is expected to be similar to a NR signal. Due to the rarity of a WIMP interaction future projects plan to use bigger xenon TPC's, based on the same idea to detect WIMP's.

## 2.4 The role of VULCAN

For the past three months I have been working on the VULCAN set up. VULCAN stands for Vacuum Ultraviolet Light Characterisation At Nikhef. The set up will be discussed in more detail in Section 3, but it has a light source which shines on a monochromator to isolate the scintillation wavelengths of xenon and argon (argon is used in DUNE, a neutrino detection experiment also using a scintillation based TPC). These isolated wavelengths then shine on the PTFE that is used in the xenon experiment and the wavelength shifting foils used in DUNE to measure properties such as fluorescence, reflectivity and transmittivity.

My role has been to characterise the intensity of the light beam at atmospheric pressure as a function of distance from the exit slit, to look at the effects of changing the exit slit of the monochromator on the intensity and to make a start with measuring the beam profile.

# 3 VUV set-up

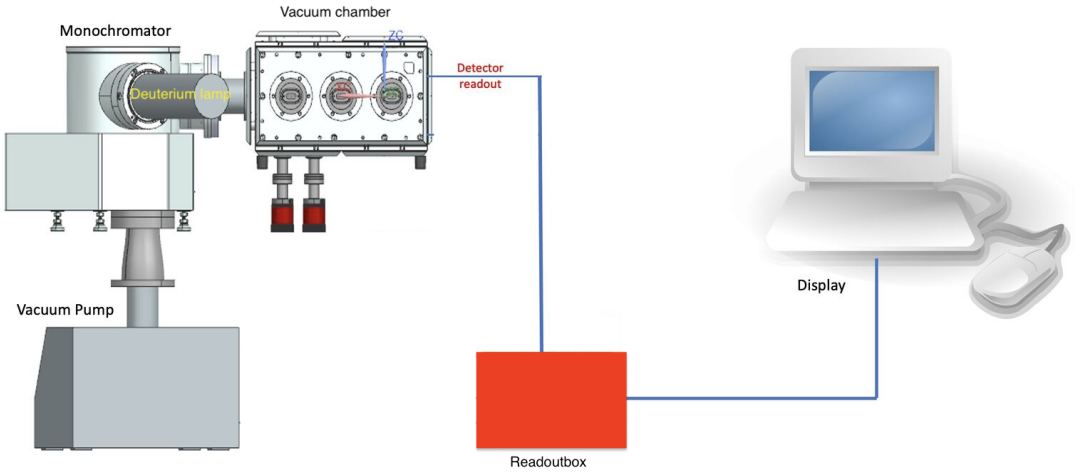


Figure 1: A simplified schematic setup of the VULCAN experiment.

Xenon and argon scintillate at wavelengths 128 and 178 nm respectively, both these wavelengths fall within the vacuum ultra violet (VUV) light range. Oxygen absorbs VUV light at normal pressure, meaning the system needs to be in a vacuum to make this light detectable. To investigate the previous named properties of materials used in scintillation based TPCs, VULCAN isolates light of these wavelengths by shining a light source with a continuous VUV spectrum on a monochromator, separating the light in its individual wavelengths. Light of a single wavelength then enters a vacuum chamber containing a sample and sensor holder. The sample holder holds the materials we want to investigate and the sensor holder holds up to three light detectors. The detected signal is amplified and then read out using a digitizer. A schematic version of the set up is shown in figure 1.

## 3.1 Light source and monochromator

### 3.1.1 Light source

The light source is a Hamamatsu deuterium lamp model L15094. A deuterium lamp has a small amount of deuterium gas that gets excited by applying a high voltage to a anode and cathode in the lamp. When the excited gas returns to its ground state the excess energy gets released in the form of photons in the VUV range, up to visible blue light. The lamp has a Magnesium Fluoride (MgF2) window because it lets through VUV light and is more durable than regular glass. This model has been chosen due to its high intensity. Figure 2 shows the emitted intensity spectrum, and a detailed description of the lamp can be found on [8].

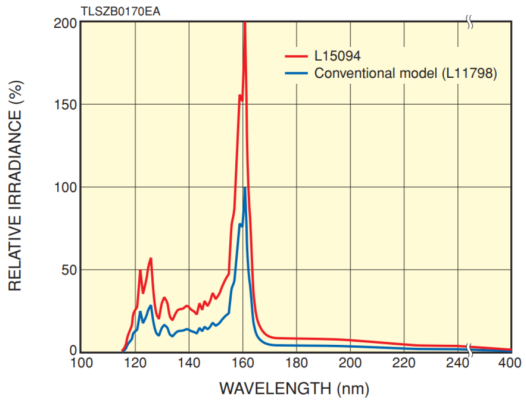


Figure 2: The intensity spectrum of the Hamamatsu L15094 Deuterium lamp compared to a conventional model [8].

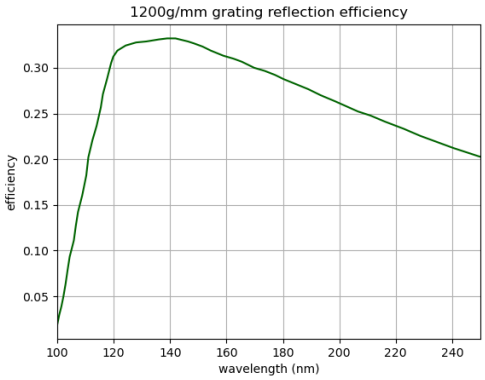


Figure 3: The reflective efficiency of the 1200 g/mm grating, provided by McPherson [9].

### 3.1.2 Monochromator

The monochromator is a McPherson 200 mm focal length vacuum monochromator model 302. It has an adjustable entrance and exit slit, but The main component of the monochromator is a 1200 grooves per mm grating, separating the light in individual wavelengths. Figure 3 shows how much the grating reflects different wavelengths of light. A grating is an instrument taking advantage of the optical phenomenon of diffraction. It has periodically spaced grooves causing phase changes based on the position [11]. These grooves act as obstacles for the incident light beam, causing constructive and destructive interference patterns in the reflected light beam. These patterns cause the light to spread out in different diffraction orders, with each order corresponding to a different wavelengths, as seen in figure 4. The formula correlating the wavelength, order, incident angle and angle of diffraction is:

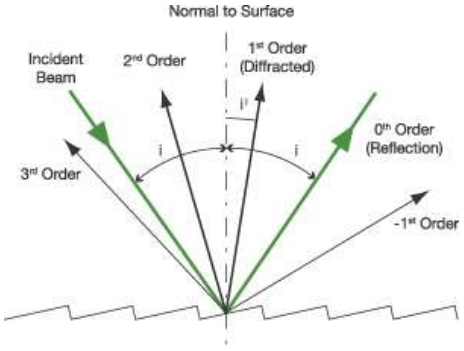


Figure 4: Schematic of diffracting light beam [10].

$$m\lambda = d(sin\theta_i \pm sin\theta_0). \quad (1)$$

This is the grating equation with $\lambda$ the wavelength, $m$ the order, $d$ the distance between the grooves, $sin\theta_i$ the angle of incidence and $sin\theta_0$ the angle of diffraction. Both angles are measured from the normal. By turning the grating individual wavelengths can be selected to exit at the exit slit. The grating can also be set to reflect all incoming light. For more detail see [9].

The entrance and exit slit are both adjustable between 0.01 and 3 mm. The entrance slit controls how much light gets inside the monochromator, and thus adjusting it changes the overall intensity of the light. The effect of changing the exit slit on the intensity is one of the things this thesis looks to investigate, but the detected light beam gets wider when the exit slit is made bigger.

## 3.2 Vacuum pump and chamber

### 3.2.1 Absorption by oxygen

VUV light gets absorbed by oxygen, the attenuation can be calculated with the following equation

$$\mu(P) = \rho(P)\sigma\frac{N_A}{M} \tag{2}$$

with $\rho(P)$ the density of oxygen in the air dependent on pressure, which can be calculated using the ideal gas law, $\sigma$ the cross section, $N_A$ Avogadro's number and M the molar mass of oxygen. After combining equation 2 with the ideal gas law we are left with

$$\mu(P) = 0.2094P\sigma\frac{N_A}{RT} \tag{3}$$

where 0.2094 is the fraction of oxygen in the air, $R$ is the universal gas constant and $T$ is the temperature. Finally the absorption can be calculated by

$$\epsilon = 100 - e^{-\mu d}. \tag{4}$$

Here the exponential is equal to the ratio $I/I_0$ with $I_0$ set to 100 and $d$ the distance the light travels. Assuming $d$ to be 30 cm and $T$ to be 293 K, the absorption spectra for 10 mbar and $10^{-5}$ mbar shown in figures 5 and 6 can be calculated.

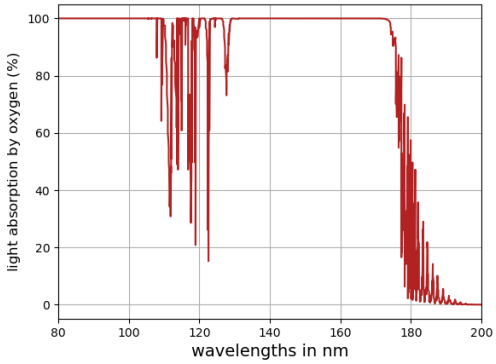


Figure 5: The absorption of VUV light by oxygen at 10 mbar.

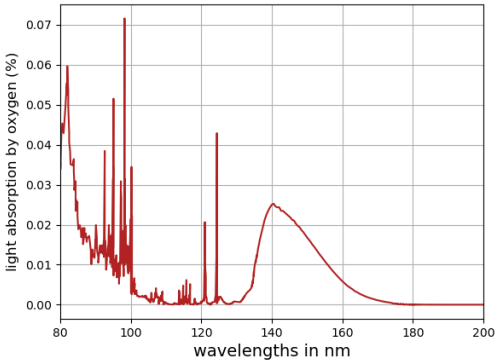


Figure 6: The absorption of VUV light by oxygen at $10^{-5}$ mbar.

### 3.2.2 Vacuum pump

To get the pressure down to a point where UV light can be observed we use a Pfeiffer vacuum pump existing of a backing pump and a turbo pump. The HiCube Eco pumping station controls both pumps and houses the backing pump, for all specifications see [12]. The backing pump is a diaphragm pump that sucks in air when the exit valve is closed and the entrance valve is opened, and pushes out the air when the exit valve is opened and the entrance valve is closed. By alternating between these two modes the pressure reduces until the backing pump is not able to reduce it anymore at which point the turbo pump takes over. The turbo pump has alternating rows of rotating and static blades with the blades pointing

in opposite direction. By rotating the rotor blades up to 1500 Hz the turbopump traps the air molecules that fall in, allowing the pressure to reduce further. Figure 7 shows an inside view of the turbo pump, with the blue dots representing air molecules.

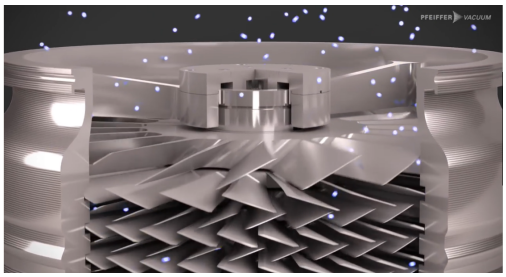

Figure 7: A inside view of the turbopump.

### 3.2.3 Vacuum chamber

The vacuum chamber is a 12 by 12 by 6 inch box consisting of a frame with individual plates attached to the frame. All the plates are sealed with O-rings, sealing the box from outside air. There are readout ports available for 9 SiPMs, a pressure gauge can be attached and it has two rotary feedthroughs that are controllable from outside the chamber. Both the sample and sensor holder are connected to these feedthourghs. The sample holder is able to hold two samples while rotating around its own axis. It is designed to either reflect the incoming light of the sample or let the light pass to directly be detected by the SiPMs. The SiPM holder is attached to a rotating arm that rotates around the sample holder to either detect the reflected light beam or directly detect in the path of the light beam. Figure 8 shows an outside view of the vacuum chamber and figure 9 shows a schematic view of how both holders are set up.

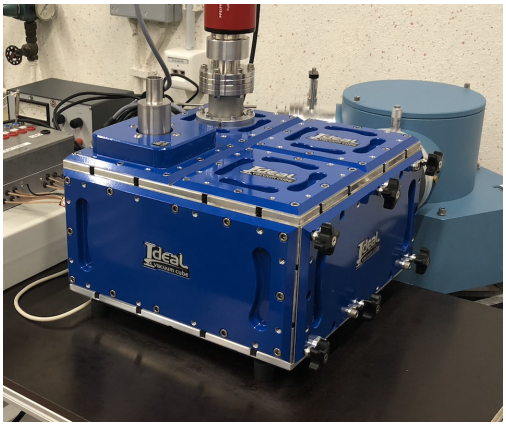


Figure 8: outside view of the vacuum chamber used in the VUV set up.

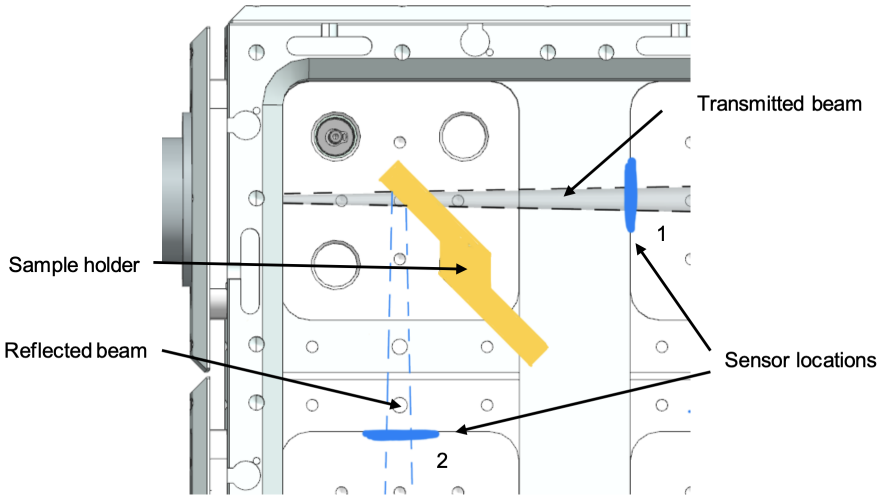


Figure 9: Inside schematic view of the arrangement of both holders.

## 3.3 SiPM

Inside the vacuum chamber silicone photomultipliers (SiPMs) are used to detect incoming light. SIPMs consist of an array of up to hunderds of thousands of single-photon avalanche diodes (SPADs) [13]. When a photon is detected the SPAD creates an electrical signal, because the SPADs are all autonomous and connected in parallel to the same read out, a single SPAD going of can be detected. This allows the SiPM to detect single photons. The SiPM has different detection efficiencies based on wavelength, see figure 10 for the efficiency across the wavelength spectrum relevant in this work.

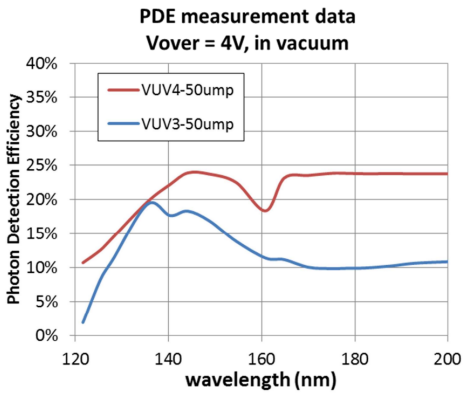


Figure 10: Efficiency spectrum of the SiPM, we use the VUV4 SiPM.

An SPAD is a reversed biased p-n junction made from silicon. To create the p-n junction both edges of the SPAD are either positively or negatively doped. A reversed bias voltage is applied to further pull apart the positive and negative regions, and to create a depletion zone in between, see figure 11. When a photon hits the depletion zone an electron-hole pair in created. If the applied reversed bias voltage is above a certain threshold called the breakdown voltage, both the electron and hole have enough energy to create secondary electron-hole pairs. The fact that electron-hole pairs can create new electron-hole pairs, is called the self sustaining avalanche process, and it ramps up the current running through the SPAD, allowing for the detection of a single photon and its time of arrival. The avalanche process is depicted in figure 12. To quench the avalanche process the SPAD is connected to a quenching circuit. This circuit lowers the bias voltage to or below the breakdown voltage, stopping the avalanche process. The reverse bias voltage must then be restored to allow for a new photon detection.

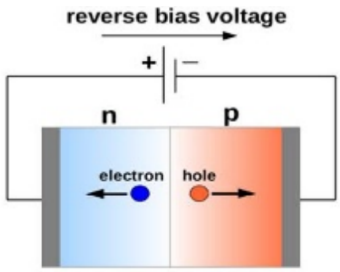


Figure 11: Schematic of the p-n junction with a reversed biased voltage [13]

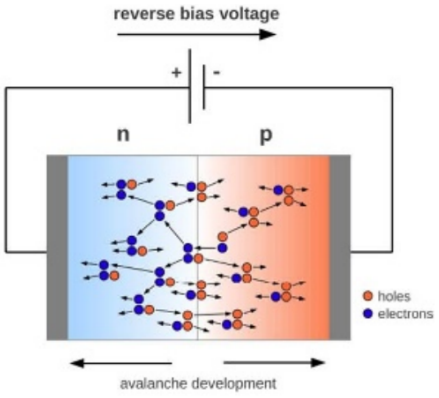


Figure 12: Schematic of the p-n junction with a reversed bias applied, showing the avalanche process [13]

The SiPMs also have a dark count rate. This is the rate at which SPADs create a signal because of thermal generations of carriers by states in the bangdap. This rate is heavily dependent on temperature, meaning high temperatures cause very high dark count rates.

# 4 Method and results

## 4.1 Sample Holder

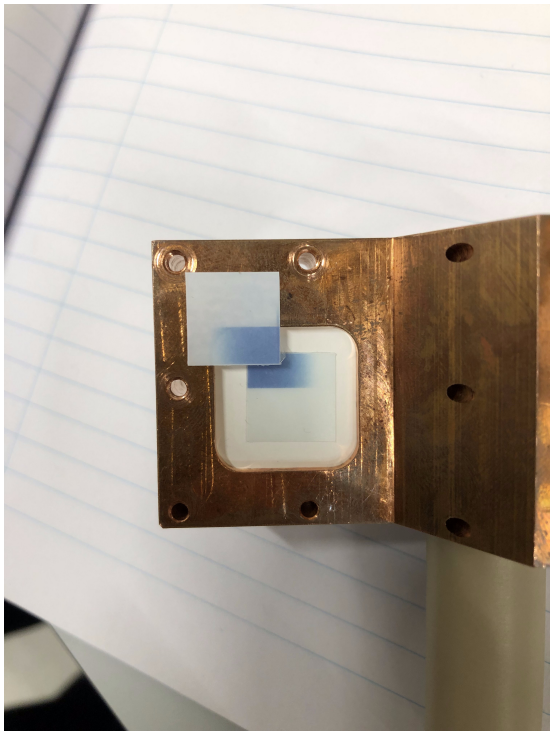

Figure 13: The location where the beam hit the sample holder before the corrections.

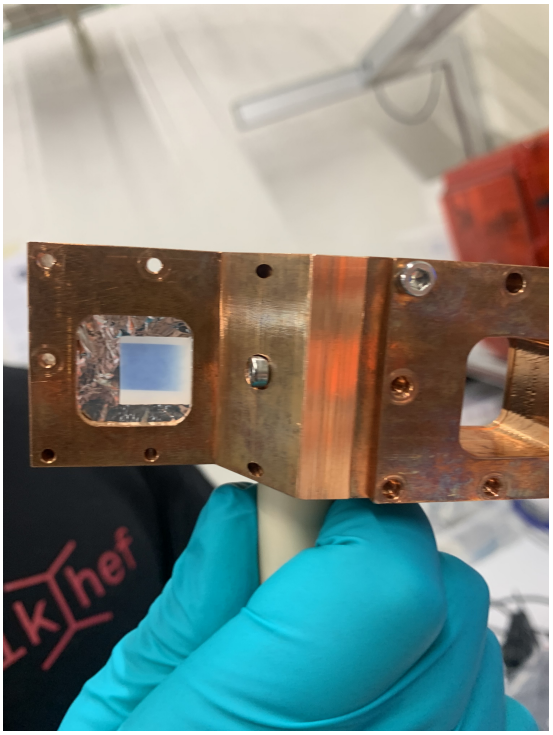

Figure 14: Location where the beam hit after the corrections were made.

To test the properties of materials used in TPC projects, the incident light beam must hit the sample in a specific way for the reflected beam to reach the detectors. Our sample holder is a copper frame with space for two samples on each sides. The holder is able to spin completely around its axis. To direct the reflected beam towards the detectors the sample holder must be turned slightly towards the beam, as seen in figure 9. This means the light beam should hit to the left of the centre of the sample, when directly in front of the light beam. This can be tested using UV sensitive paper, which turns blue when exposed to UV light. Figure 13 shows where the light beam was hitting the sample. To correct for these discrepancies the frame of the sample holder was raised 6 mm and it was widened 7 mm from the centre, figure 14 shows where the light beam hit after corrections.

## 4.2 From data to intensity

The voltage the SiPMs detect is converted to ADC counts by the digitizer. The measured data is therefore ADC counts versus time, and is called a trace. ADC counts

can be converted back to voltage based on the amount of bits. To calculate the intensity from a trace, two techniques are used, the first one determines the total charge by integrating the measured voltage over time, the second one finds peak in the recorded traces. Figure 15 shows a high intensity measurement, to calculate the total charge, the baseline is set to 0, and the ADC counts are converted to voltage, see figure 16. By integrating over time, the total charge is then acquired. The other technique counts the amount of peaks found within the trace, see figure 17. every data point is the average of 5000 measurements with the same parameters, the errors are the standard deviation. The counting peaks method is unable to take into account the height of the peak, while integration does not account for overlapping areas that only show peaks. This creates the expectation that the integration method would work better in traces with multiple photon detections at the same time, while counting peaks would prefer traces with single photon detections.

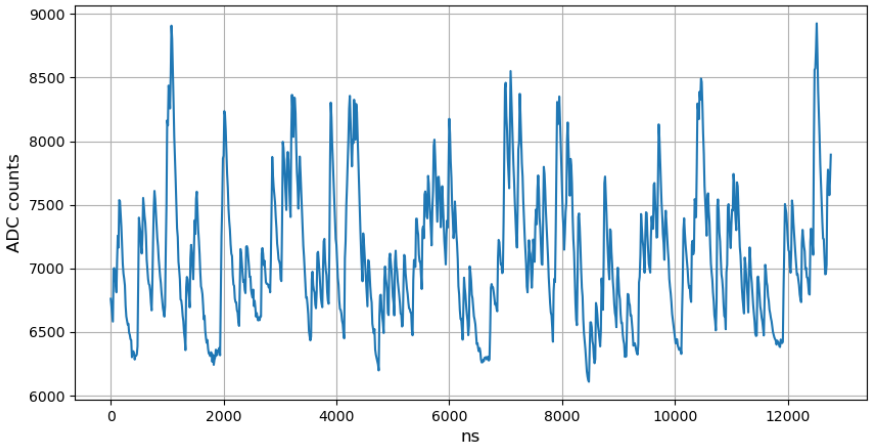


Figure 15: Raw data of measurement at 4.5cm, exit slit at 1 mm, N = 3456.

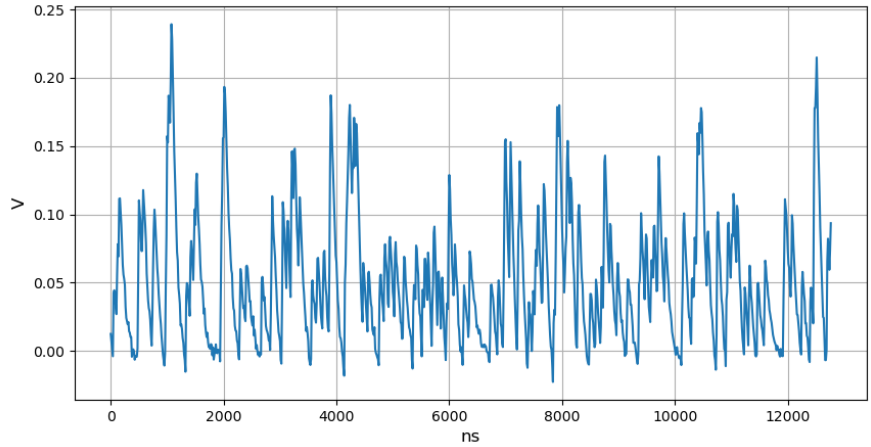


Figure 16: Baseline corrected data of measurement at 4.5cm, exit slit at 1 mm, N = 3456.

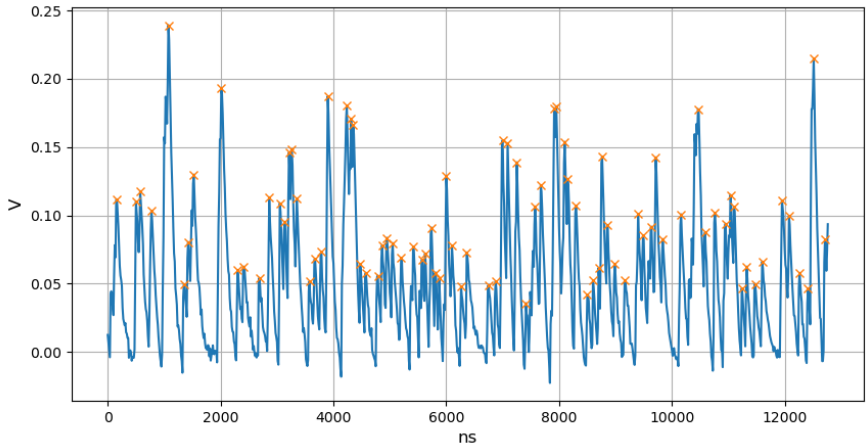


Figure 17: baseline corrected data with peaks highlighted of measurement at 4.5cm, exit slit at 1 mm, N = 3456.

## 4.3 Corrected Light Spectrum

To completely understand the acquired results, we must understand how certain parts of the set up influence the measured intensity. The measured intensity can be corrected for these influences, after which the measured intensity spectrum can be compared to the provided intensity profile, figure 2. The first intensity affecting part is the entrance slit, but the entrance slit adjusts the overall intensity of the incoming light, meaning it only scales the measured intensity spectrum and thus its affects are not taken into account. The grating efficiency, figure 3, reflects different wavelengths with different efficiencies, hence it must be accounted for. The next step would be to take into account the air attenuation, but for measurements in vacuum at the wavelengths of interest this is $\approx 0$. The final intensity affecting component is the SiPM efficiency, figure 10. These corrections can now be applied to an intensity spectrum, computed from data taken before the start of this bachelor project. Figure 18 shows the computed values. Figure 19 and 20 show the data corrected for the SiPM and grating respectively and figure 21 shows the spectrum corrected for both. Figure 22 shows the corrected data compared to the lamp spectrum.

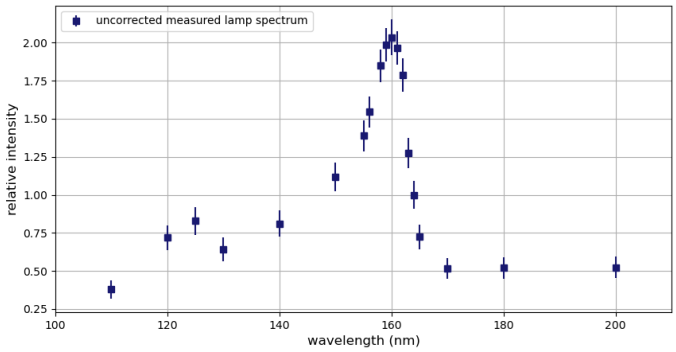


Figure 18: Uncorrected measured intensity profile in vacuum, normalised to 164 nm.

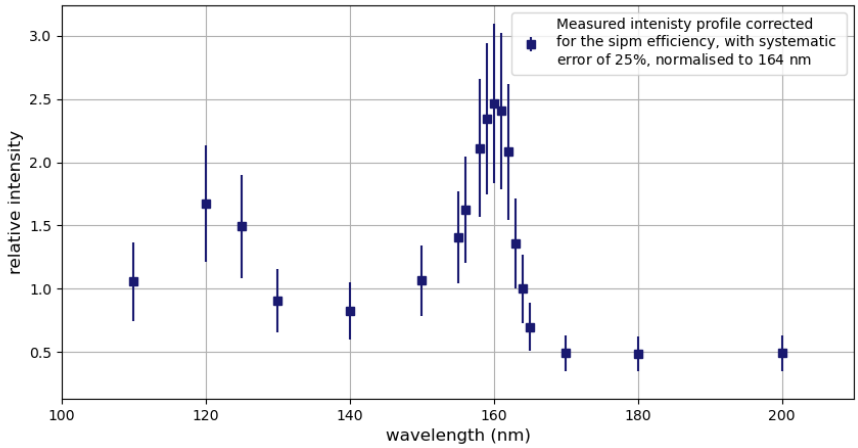


Figure 19: SiPM corrected in vacuum measured intensity profile, normalised to 164 nm.

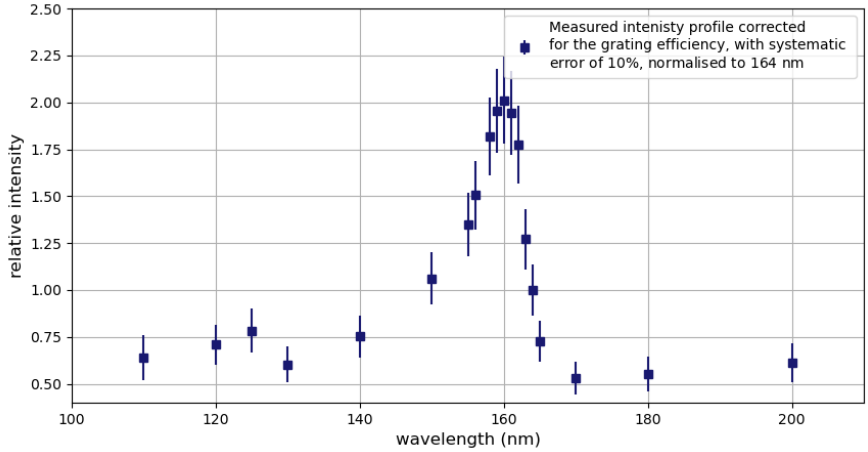


Figure 20: Grating corrected in vacuum measured intensity profile, normalised to 164 nm.

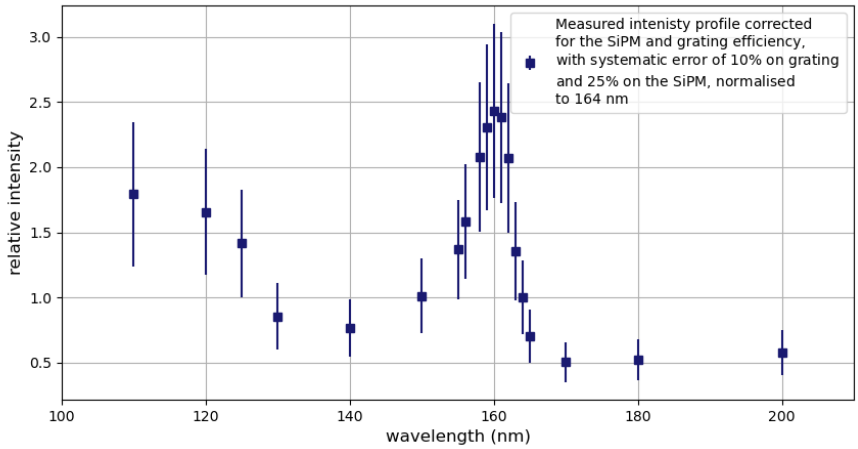


Figure 21: In vacuum measured intensity profile corrected for grating and SiPM efficiency, normalised to 164 nm.

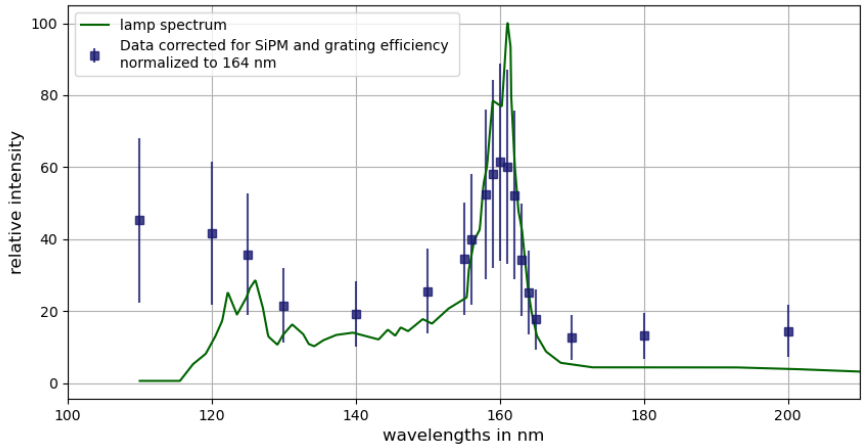


Figure 22: In vacuum measured intensity profile corrected for grating and SiPM efficiency, normalised and scaled to 164 nm.

## 4.4 Angle of detection

If the SiPM and incoming light beam are not perpendicular, the surface with which the SiPM is able to detect light becomes smaller, which consequently decreases the measured intensity. Figure 23 shows the relative intensity measured versus the angle between the SiPM and light beam. The relative intensity is equal to the component of the surface perpendicular to the light beam at an angle. This component can be calculated with 5. Where $S$ is the surface of the SiPM and $S_{eff}$ the perpendicular component of the surface at angle $\theta$.

$$S_{eff} = \cos\theta S. \tag{5}$$

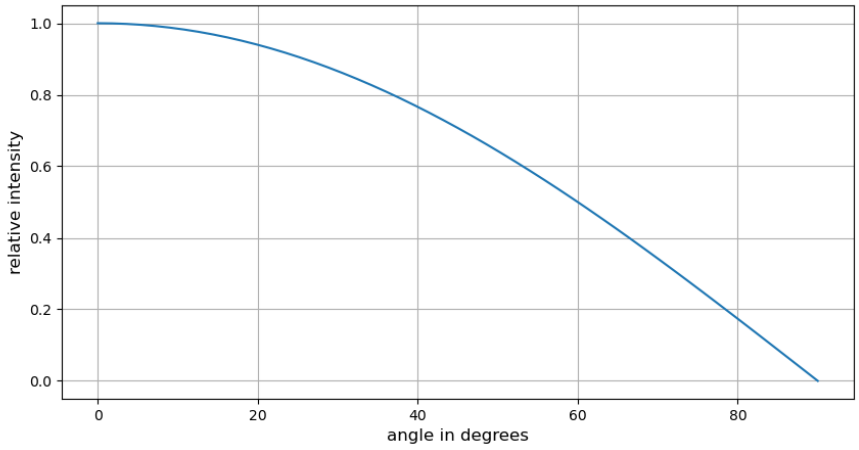


Figure 23: Relative intensity calculated between 0 and 90 degrees.

## 4.5 Distance characterisation

When measuring either the reflected or transmitted beam, the distance travelled by the light beam differs. To measure the influence of this difference on the inten-

sity, the intensity was measured at different distances. We expect this relation to be quadratic since the detector surface stays the same, while the light beam propagates. The intensity was measured by removing the SiPM holder from the rotating arm placed in a piece of metal that could be moved towards and away from the exit slit. All these measurements have been done in air with the monochromator on the reflective setting, because the correlation between distance and intensity is not affected by different wavelengths. All the measurements are done with exit slit values of 1, 2 and 3 mm, and the entrance slit on 0.02 mm. Figure 24 and 25 show the data processed using the integration method and a quadratic fit through the 2 mm exit slit points. Figure 26 and 27 show the data and fit through the 2 mm exit slit values using the peak counting method. Both fits are fitted to equation 6 with the found fit values in table 1.

$$y = ax^2 + bx + c \tag{6}$$

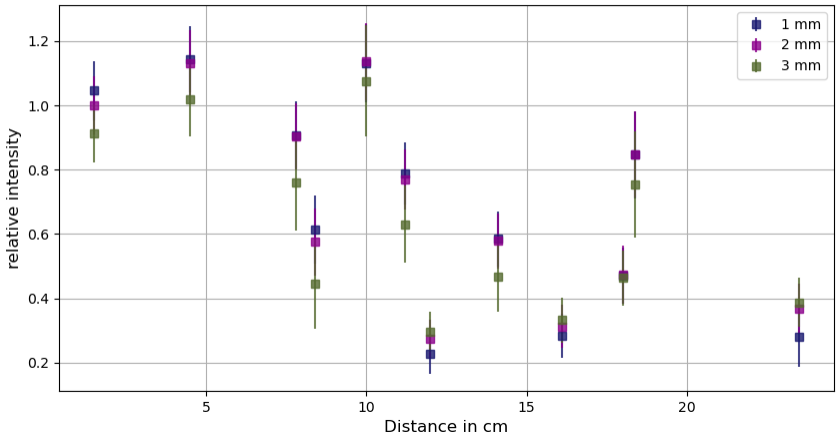


Figure 24: Distance characterisation with exit slit at 1, 2 and 3 mm, using the integration method.

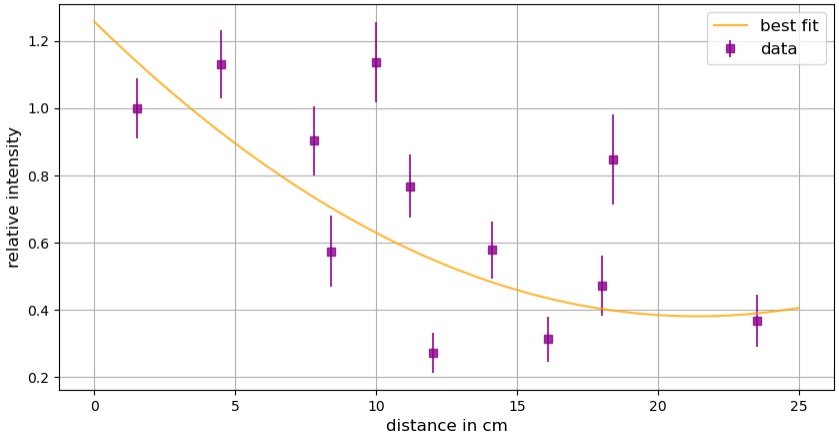


Figure 25: Quadratic fit through the values with exit slit at 2 mm, using the integration method.

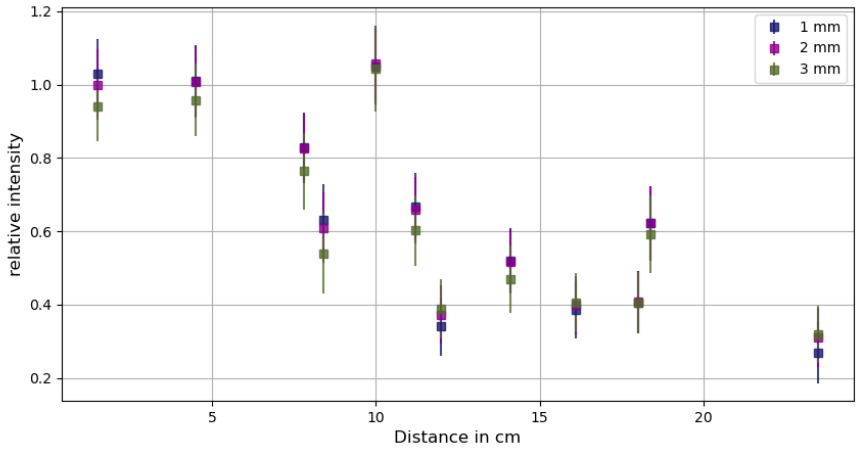


Figure 26: Distance characterisation with exit slit at 1, 2 and 3 mm, using the counting peaks method.

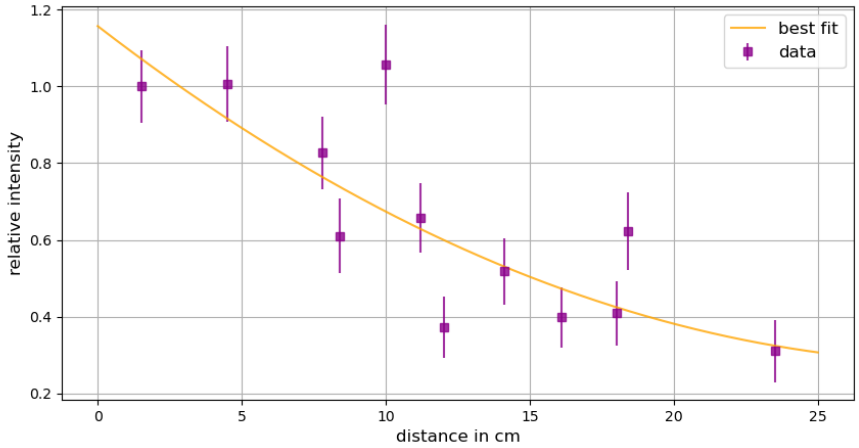


Figure 27: Quadratic fit through the values with exit slit at 2 mm, using the counting peaks method.

| parameters | integration | error | counting peaks | error |
|---|---|---|---|---|
| a | $1.92 * 10^{-3}$ | $\pm 1.61 * 10^{-3}$ | $9.55 * 10^{-4}$ | $\pm 1.11 * 10^{-3}$ |
| b | $-8.20 * 10^{-2}$ | $\pm 4.26 * 10^{-2}$ | $-5.79 * 10^{-2}$ | $\pm 2.94 * 10^{-2}$ |
| c | 1.26 | $\pm 0.27$ | 1.16 | $\pm 0.18$ |
| reduced $\chi^2$ | 7.88 | - | 3.38 | - |

Table 1: Table with the fit values for the integration and counting peaks method.

## 4.6 Measuring with multiple SiPMs

A big step in the further improvement of the VULCAN setup is being able to measure with multiple SiPMs simultaneously, to characterise the beam profile. The current sample holder can hold up to three SiPMs at the same time, see figure 28 to see the arrangement. The read out has enough connections to read out nine SiPMs at the same time, so in the future more SiPMs can be used simultaneously. While measuring with three SiPMs read out channel three only showed high electrical noise, giving an undetectable signal. This is most likely because of the connection to the read out, because the SiPM in channel three did give a signal in a different channel, and other SiPMs also did not give a signal in channel three. The baseline corrected data of a dark count measurement with two SiPMs is shown in figure 29.

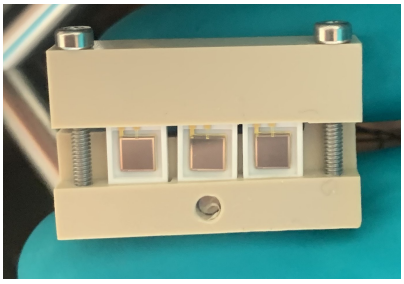

Figure 28: Three SiPMs inside the sensor holder, right SiPM connected to channel one, middle SiPM connected to channel 2, left SiPM connected to channel three.

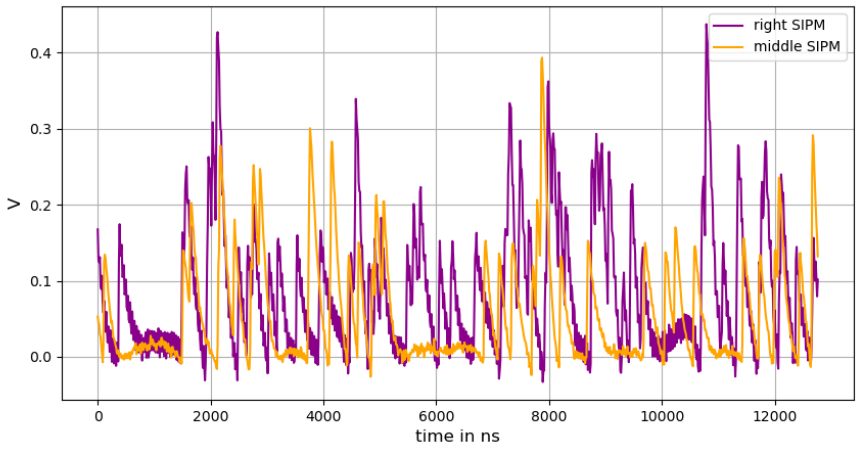


Figure 29: Baseline corrected darkcount measurement with 2 SiPMs in vacuum.

# 5 Discussion

## 5.1 interpreting results

Figure 18 shows the acquired light spectrum, figure 19 and 20 show the data corrected for the SiPM and grating individually and figure 21 shows both the corrections together. When comparing the grating corrected spectrum with the uncorrected spectrum, the grating corrected spectrum only shows slight changes. Looking at figure 3 this slight change is all we would expect, because the efficiency between 120 and 170 nm is very similar. This means the region where the measured intensity shows substantial differences, the applied correction is roughly the same for all values. The regions outside the range 120 to 170 nm show a slight increase, which also is expected because the grating efficiency is lower in those regions. When

looking at the SiPM corrected spectrum the relative intensity increases around 160 nm and the values below 140 nm increase significantly, this is again in line with expectations when looking at the sipm efficiency, figure 10. Here we can see the efficiency is fairly constant, except around 160 nm and below 140 nm, where the efficiency is lower, resulting in a higher relative intensity. Figure 22 shows the corrected spectrum compared to the provided lamp spectrum, due to big uncertainties on the SiPM and grating efficiency the error bars are big, but both specrta still show a resemblance, apart from the peak around 160 nm and the values below 120 nm. The cut off at the peak is most likely due to the SiPMs not being able to detect more light. The values for lower wavelengths increase substantially due to the applied corrections. There is no provided value for SiPM efficiency at 110 nm, so the applied correction is an interpolated value and the grating efficiency is $\approx 0.15$. Correcting for these small values causes the relative intensity to increase.
The intensity measurements at different distances, Figure 24 and 26, both show a similar trend, agreeing with the expectation of a quadratic relation. Both figures also show some points that lay far off the best fit. These discrepancies are most likely due to problems with the set up during measurements, because both techniques show the same irregularities. Both techniques show similar results, while the values found using the counting peaks method are closer together, resulting in a better fit. The counting peak method does not take into account simultaneous SPAD photon detection, meaning only more peaks account for higher intensities, this might be why the determined intensities using counting peaks are relatively closer together.
Looking at the intensities for different exit slit values in figure 24 and 26, almost all distances show the measurements at an exit slit value of three mm, give lower intensities then at exit slit values one or two mm. Since both techniques show the same discrepancies, this is probably not a computational error. With the lowest exit slit value of one mm and wavelengths between 100 and 200 nm, diffraction does not play a big enough role to cause this effect. A different explanation might be the propagation of the light beam at high exit slit values. If three mm exit slit would cause the light beam to widen to more than the surface of the SiPM, the SiPM would detect less of the total light compared to having the exit slit at low values, where the entire light beam would hit the SiPM surface. At high distances the beam would be widened for all exit slit values, explaining why the intensities lay closer together at these distances.
Figure 29 shows a simultaneous dark count measurement for two SiPMs. This is more than expected from a dark count measurement, meaning the acquired data is not reliable for intensity calculations, and thus not usable for characterising the beam profile. But, it does show multiple SiPMs can be used and read out simultaneously.

## 5.2 Further improvements

The VULCAN setup has a couple of improvements it can make, one is using vacuum compatible female D-subs inside the vacuum chamber to connect the SiPMs with the read out system. This would replace trying to fit very small pins on male D-subs inside the vacuum chamber by placing the pins inside the female D-sub outside the vacuum chamber and just fitting the male and female D-sub together inside

the vacuum chamber. An example of a compatible D-sub can be found on [14].
A further improvement can be made regarding the electrical noise caused by the electronics connecting the vacuum chamber to the read out system. New noise blocking paper and protection has been bought, but the paper does not show a significant difference and the casing does not fit without having to completely take apart the connections and rebuilding them with the casings.
Besides buying new accessories to improve the set up, some improvements can be made regarding the distance characterisation, for example mounting the detectors to a fixed rail in front of the beam, completely eliminating the possibility that the SiPMs are not perpendicular to the incoming beam. For measurements regarding the reflectivity or transmittivity of different materials a system fixing the sample and sensor holder angles should be looked at. This would eliminate the process of calibrating every time a measurement needs to be done, and guarantees the SiPMs are in the middle of the reflected or transmitted light beam.

# 6 Conclusion

The goal of this bachelor project was to further prepare the VULCAN set up for eventual material property measurements on the materials used in the scintillation based TPCs of XENONnT and DUNE. This is done by identifying and correcting for parts of the set up that have an influence on the intensity profile, by looking at the relation between relative intensity and distance to the exit slit, by looking at the relation between exit slit width and intensity, and by profiling the light beam through measuring with multiple SiPMs simultaneously. The corrected intensity profile shows big error bars due to the large uncertainties on the applied corrections, but the provided lamp spectrum can be recognised if the assumptions are made that the SiPMs are not able to detect the amount of light coming in around 160 nm, and that the high corrected intensities at low wavelengths are a result of low, unreliable correction values. The relation between relative intensity and distance can be seem as quadratic when using the integration and counting peaks methods to calculate the intensity. Counting peaks provides the best fit from the two techniques, but the errors on the found fit values are big for both fits. Measurements done with multiple SiPMs simultaneously, trying to profile the light beam, were not reliable due to dark counts measurements being higher than expected. It does show multiple SiPMs can be read out at the same time, meaning the profile of the light beam can be acquired, if the data is reliable. All in all, small steps have been taken to prepare the VULCAN set up to fulfil its role in the search for an answer to one of the biggest questions in modern day physics, does dark matter exist?

# 7 Acknowledgements

I would like to thank the entire dark matter group. Everyone, independent of their role within the group, was always willing to answer questions and help when problems arose. I would like to thank Marjolein van Nuland and Tina Pollmann in particular, for supervising this project and always being available whenever help was needed.

# References

[1] F. Zwicky, Die Rotverschiebung von extragalaktischen Nebeln, *Helv. Phys. Acta* **6**, 110 (1933).

[2] V. C. Rubin, J. Ford, W. Kent, Rotation of the Andromeda Nebula from a Spectroscopic Survey of Emission Regions, **159**, 379 (1970).

[3] D. Clowe, *et al.*, A direct empirical proof of the existence of dark matter*, *The Astrophysical Journal* **648**, L109 (2006).

[4] V. Springel, *et al.*, Simulations of the formation, evolution and clustering of galaxies and quasars, **435**, 629 (2005).

[5] Tisserand, P., *et al.*, Limits on the macho content of the galactic halo from the eros-2 survey of the magellanic clouds, *A&A* **469**, 387 (2007).

[6] L. Roszkowski, E. M. Sessolo, S. Trojanowski, WIMP dark matter candidates and searches—current status and future prospects, *Reports on Progress in Physics* **81**, 066201 (2018).

[7] E. Aprile, *et al.*, Projected WIMP sensitivity of the XENONnT dark matter experiment, *Journal of Cosmology and Astroparticle Physics* **2020**, 031 (2020).

[8] Hamamatsu, L15094. `https://www.hamamatsu.com/us/en/product/manufacturing-support-systems/electrostatic-remover/vuv-ionizer/L15094.html`, Accessed between April and June 2023.

[9] McPherson, Mcpherson 234/302. `https://mcphersoninc.com/pdf/234302.pdf`, Accessed between April and June 2023.

[10] Andor, Oxford instruments (2020). `https://andor.oxinst.com/learning/view/article/diffraction-gratings`, Accessed between April and June 2023.

[11] D. R. Paschotta, Rp photonics. `https://www.rp-photonics.com/diffraction_gratings.html`, Accessed between April and June 2023.

[12] Pfeiffer, Hicube 80 eco. `https://www.pfeiffer-vacuum.com/en/products/vacuum-generation/pumping-stations/turbo-pumping-stations/hicube-eco/20017/hicube-80-eco-dn-40-iso-kf-mvp-015-4`, Accessed between April and June 2023.

[13] S. Gundacker, A. Heering, The silicon photomultiplier: fundamentals and applications of a modern solid-state photon detector, *Physics in Medicine & Biology* **65**, 17TR01 (2020).

[14] Allectra, Sub-d 9-way hv socket, female. `https://shop.allectra.com/products/211-FS09-HV-V2`, Accessed between April and June 2023.